Modeling of resistance characteristics of a continuously-graded distributed Bragg reflector in a 980-nm vertical-cavity surface-emitting laser*

Huang Meng(黄 梦)[a)], Wu Jian(吴 坚)[a)†], Cui Huai-Yang(崔怀洋)[a)], Qian Jian-Qiang(钱建强)[a)], and Ning Yong-Qiang(宁永强)[b)]

[a)] *Department of Applied Physics, Beihang University and Key Laboratory of Micro-Nano Measurement-Manipulation and Physics (Ministry of Education), Beijing* 100191, *China*

[b)] *State Key Laboratory of Luminescence and Applications, Changchun Institute of Optics, Fine Mechanics and Physics, Chinese Academy of Sciences, Changchun* 130033, *China*

(Received 7 March 2012; revised manuscript received 18 April 2012)

The resistance characteristics of a continuously-graded distributed Bragg reflector (DBR) in a 980-nm vertical-cavity surface-emitting laser (VCSEL) are modeled in detail. The junction resistances between the layers of both the p- and n-DBR mirrors are analysed by combining the thermionic emission model and the finite difference method. In the meantime, the intrinsic resistance of the DBR material system is calculated to make a comparison with the junction resistance. The minimal values of series resistances of the graded p- and n-type DBR mirrors and the lateral temperature-dependent resistance variation are calculated and discussed. The result indicates the potential to optimize the design of the DBR reflectors of the 980-nm VCSELs.

Keywords: distributed Bragg reflector (DBR), resistance characteristics, vertical-cavity surface-emitting lasers

PACS: 42.55.Px, 73.40.Kp, 73.40.Cg **DOI:** 10.1088/1674-1056/21/10/104207

1. Introduction

In the development of a high power, single 980-nm vertical-cavity surface-emitting laser (VCSEL) diode, the resistance of the VCSEL, and particularly the resistance of the distributed Bragg reflector (DBR), play a very important role in the performance of the device, as these resistances lead to a considerable thermal effect in the VCSEL. Thus, to enhance the VCSEL power and improve the device characteristics, such as threshold current reduction, the derivation of low-order optical modes, etc., the continuously-graded DBR mirrors have been proposed and used for VCSELs in the last decade to minimize the influence of resistance.

However, it is usually difficult to accurately determine the graded DBR resistance by experimental measurements. Instead, modeling is a more popularly-used approach to the assessment of the resistance characteristics of the graded DBR. Thus, some models on how to calculate and determine the graded DBR resistances have been proposed[1−10] in the past. Unfortunately, the published modeling work concerning the continuously-graded DBRs presented insufficient calculation and analysis due to the fact that too many approximations or simplification treatments were used, and typically, the neglect of n-type of DBR resistance. Up to now, it is still hard to directly use the previous models and results for an exact assessment of resistance influence from continuously-graded DBRs for high power 980-nm VCSELs. In addition, previous studies are also lacking in discussion about the temperature-induced resistance variation from graded DBR mirrors, however this is important for exactly characterizing the DBR resistance properties.

In this paper, we start with modeling both the intrinsic and the junction resistance characteristics of the continuously-graded $Al_xGa_{1-x}As$ p- and n-DBR mirrors for high power 980-nm VCSELs in sufficient detail by combining the thermionic emission model and the finite difference method. Then, the temperature dependence and the distribution of these resis-

*Project supported by the National Natural Science Foundation of China (Grant No. 10974012).

†Corresponding author. E-mail: jwu2@buaa.edu.cn

© 2012 Chinese Physical Society and IOP Publishing Ltd

tances are calculated and discussed.

2. Intrinsic resistance of the DBR material system

The DBR structure and material system of the VCSEL for the model are based on the experimental sample of a 980-nm bottom-emitting VCSEL with an output power of 1.0 W. The top and bottom DBR reflectors consist of 30 periods of the continuously-graded p-type $Al_xGa_{1-x}As/Al_{1-x}Ga_xAs$ pairs with a thickness of 0.02 μm per layer ($0.1 \leq x \leq 0.9$, a carbon-doping concentration of 2.5×10^{18} cm^{-3}) and 28-periods of continuously-graded n-type $Al_xGa_{1-x}As/Al_{1-x}Ga_xAs$ pairs with a thickness of 0.02 μm per layer ($0.1 \leq x \leq 0.9$, and a silicon-doping concentration of 2.0×10^{18} cm^{-3}), respectively. The active region consists of two $Ga_{0.8}In_{0.2}As$ quantum wells between which a $GaAs_{0.92}P_{0.08}$ layer is sandwiched. The device is grown on a GaAs substrate. The L–I–V characteristics of the sample are plotted in Fig. 1.

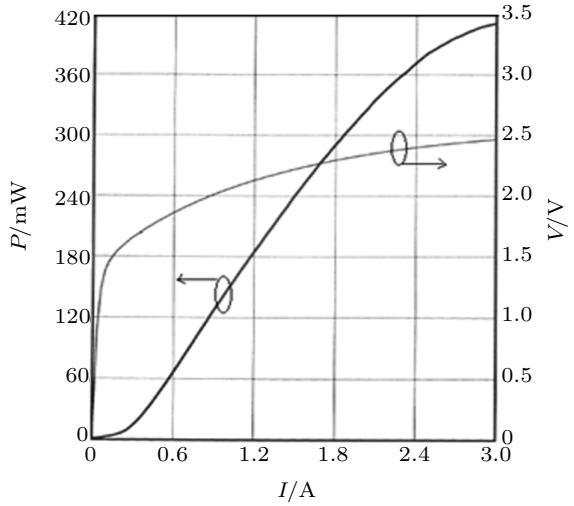


Fig. 1. The L–I–V characteristics of the 980-nm VCSEL.

The intrinsic resistivity of the semiconductor material can be expressed as[10]

$$\rho(N_{e,h}, T) = \frac{1}{q \times \mu_{e,h} \times N_{e,h}}, \tag{1}$$

where T and q are the temperature and the electric charge, respectively, $\mu_{e,h}$ is the mobility of electrons or holes in the material, and $N_{e,h}$ denotes the carrier concentration. In terms of Matthiesen's rule, the carrier mobility of $Al_xGa_{1-x}As$ can be determined by

$$\frac{1}{\mu_{e,h}} = \frac{1}{\mu_{e,h}(N_{e,h}, T)} + \frac{1}{\mu_{e,h}(x)}, \tag{2}$$

where $\mu_{e,h}(N_{e,h}, T)$ is the carrier mobility relating to the ionized-impurity scattering and the lattice scattering, and $\mu_{e,h}(x)$ is the carrier mobility depending on the mole fraction, x of aluminum, which is called alloy scattering and given by[10]

$$\mu_{e,h}(x) = \frac{(2\pi)^{1/2} q \hbar^4 N_{al}}{(kT)^{1/2} (m^*_{e,h})^{1/2} x(1-x) \Delta U^2}. \tag{3}$$

In Eq. (3), $m^*_{e,h}$ denotes the effective mass of the electron and hole, expressed respectively as $m^*_e = (0.0667 + 0.0835x)m_0$ and $m^*_h = (0.34 + 0.412x)m_0$ with m_0 being the rest mass of the electron; $\hbar = h/2\pi$, with h being the Planck constant; N_{al} denotes the density of alloy sites, which is 4.46×10^{22} cm^{-3} here; ΔU is the bandgap difference between $Al_xGa_{1-x}As$ and GaAs materials and written as

$$\Delta U = E_{g,Al_xGaAs} - E_{g,GaAs}. \tag{4}$$

Here, the bandgap of the $Al_xGa_{1-x}As$ material can be expressed as[11]

$$E_{g,Al_xGaAs} = \begin{cases} 1.424 + 1.247x, & x < 0.5, \\ 1.424 + 1.247x + 1.147(x - 0.5)^2, & x > 0.5. \end{cases} \tag{5}$$

Provided that the doped impurity is fully ionized in the material, its concentration may be treated as a free carrier concentration. With Eqs. (1)–(5), the mean of the intrinsic resistivity over $x \in (0.1, 0.9)$ for the graded p- and n-type $Al_xGa_{1-x}As$ materials at $T = 300$ K are obtained to be 0.03714 Ω·cm and 0.00125 Ω·cm, respectively.

3. Junction resistance between graded DBR layers

Since a bandgap difference exists between the two layers which have different x values in the DBR mirror, an isotype hetero-junction containing the carrier accumulation and depletion regions separately on each side of the junction occurs between the layers. The accumulation and depletion regions for electrons in the n–n junction are formed at the narrower bandgap (NBG) and the broader bandgap (BBG) sides of the junction, respectively. Similarly, the accumulation and depletion regions for holes in the p–p junction are generated at the BBG and NBG sides, respectively. Thus, a weak built-in electric field is generated, owing to the same doping concentrations of the impurity in both the NBG and BBG regions of the isotype hetero-junction. In this case, when a reverse-bias voltage

is applied to the junction, the injection carriers have to overcome an additional barrier generated from the bandgap difference to pass through the junction. This is called the junction resistance of the DBR, which occurs in all pairs of the DBR layers. The relevant energy-band structures of the DBRs are illustrated in Fig. 2.

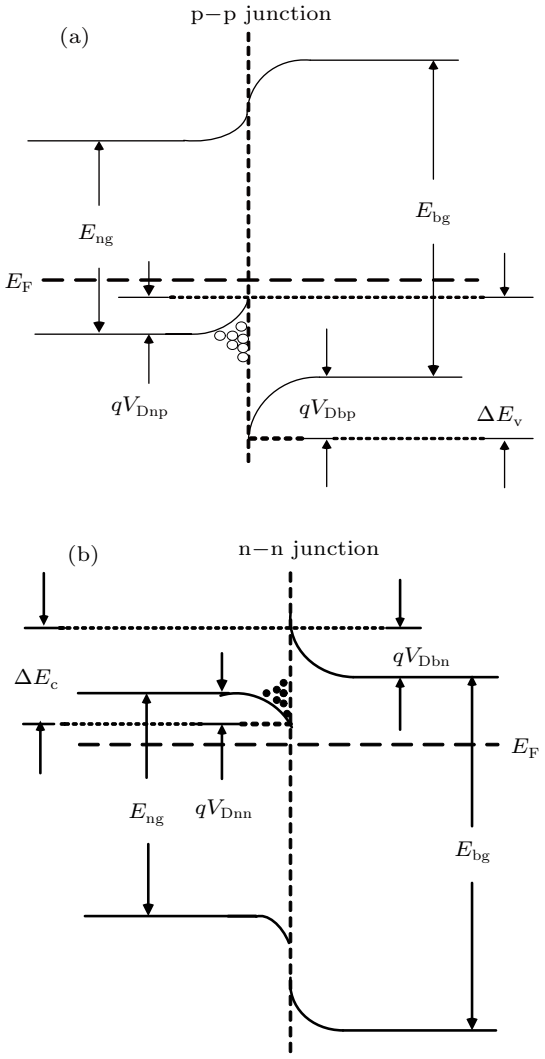


Fig. 2. Energy-band structures of the isotype hetero-junctions, (a) the p–p junction and (b) the n–n junction.

Obviously, there are two isotype hetero-junctions generated in one pair of $Al_xGa_{1-x}As$ DBR layers, to which the reverse-bias and the forward-bias voltages are applied, respectively, due to the alternative variations of $x = 0.1 \to 0.9$ and $0.9 \to 0.1$ from the different DBR layers.

In the model, the finite difference method is used to characterize the resistance of one $Al_xGa_{1-x}As$ DBR layer with the continuous variation of x-value or the bandgap. In this way, one layer of the DBR mirror may be divided into a number of discrete transitional sub-layers by $\Delta x = (0.9 - 0.1)/n$ here, and thus, the continuous x-values are converted into a series of discrete graded values corresponding to the different transitional sub-layers so that the theory on the abrupt bandgap difference of the isotype-hetero-junction can be used for the continuous bandgap difference case. In addition, the thermionic emission model is used in the DBR resistance analysis here due to the same doping concentrations of the impurity on both the NBG and BBG sides of the junction in the DBR mirror, so that the carrier diffusion effect in the junction would be weaker than the thermionic emission influence, particularly for the high power operation of 980-nm VCSELs.

3.1. Junction resistance of graded p-DBR

As analysed above, the junction resistance in one pair of p-DBR layers consists of two parts corresponding to the reverse-bias and the forward-bias voltages, respectively. With the thermionic emission model,[12] the current density on the junction can be expressed as

$$J_{\rm fp,rp} = \pm qN_{\rm bp}\Big(\frac{kT}{2\pi m_{\rm h}^*}\Big)^{1/2}\exp\Big(-\frac{qV_{\rm Dbp}}{kT}\Big) \times\Big[\exp\Big(\pm\frac{qV_{\rm bp}}{kT}\Big) - \exp\Big(\pm\frac{qV_{\rm np}}{kT}\Big)\Big], \quad (6)$$

where $J_{\rm fp}$ and $J_{\rm rp}$ denote the current densities at the forward-bias and the reverse-bias junctions, respectively, which correspond to the symbols "+" and "−" in Eq. (6); $V_{\rm bp}$ and $V_{\rm Dbp}$ are the applied voltage and the generated built-in voltage on the BBG side of the junction, respectively; $V_{\rm np}$ is the voltage applied to the NBG side of the junction.; $N_{\rm bp}$ is the carrier concentration in the BBG region and approximately equal to the impurity concentration in the material. As the scattering carriers (electrons or holes) are always accumulated in the NBG region of the isotype hetero-junction, there appears to be a better current conductivity or less resistance in the NBG layer. Thus, the applied voltage of the junction will mostly drop into the depletion region of the BBG layer. So equation (6) can be rewritten as follows by omitting the voltage drop into the NBG region of the junction:

$$J_{\rm fp,rp} = \pm qN_{\rm bp}\Big(\frac{kT}{2\pi m_{\rm h}^*}\Big)^{1/2}\exp\Big(-\frac{qV_{\rm Dbp}}{kT}\Big) \times\Big[\exp\Big(\pm\frac{qV_{\rm bp}}{kT}\Big) - 1\Big]. \quad (7)$$

In terms of the Ohm's law, the differential resistance is written by

$$\rho'_{\rm p} = RA = \frac{{\rm d}V_{\rm bp}}{{\rm d}J}, \tag{8}$$

where R is the resistance and A is the area through which the current flows. Substituting Eq. (7) into Eq. (8) yields

$$\rho'_{\rm fp,rp} = \left\{\frac{q^2 N_{\rm bp}}{kT}\left(\frac{kT}{2\pi m^*_{\rm h}}\right)^{1/2}\right\}^{-1} \times \exp\left[\frac{q(V_{\rm Dbp} \mp V_{\rm bp})}{kT}\right]. \tag{9}$$

In order to solve Eq. (9), the following relations have to be satisfied for the p–p junction:[13]

$$\frac{\exp(\beta_{\rm np}) - \beta_{\rm np} - 1}{\exp(-\beta_{\rm bp}) + \beta_{\rm bp} - 1} = \frac{\varepsilon_{\rm b} N_{\rm bp}}{\varepsilon_{\rm n} N_{\rm np}} = \frac{\varepsilon_{\rm b}}{\varepsilon_{\rm n}}, \tag{10}$$

$$\beta_{\rm np} = \frac{qV_{\rm Dnp}}{kT}, \tag{11}$$

$$\beta_{\rm bp} = \frac{q(V_{\rm Dbp} - V_{\rm bp})}{kT}, \tag{12}$$

$$\beta_{\rm p} = \frac{q(V_{\rm Dp} - V_{\rm p})}{kT}, \tag{13}$$

$$q(V_{\rm Dp} - V_{\rm p}) = \Delta E_{\rm F}, \tag{14}$$

$$V_{\rm Dnp} + V_{\rm Dbp} = V_{\rm Dp}, \tag{15}$$

where $V_{\rm p}$ and $V_{\rm Dp}$ denote the applied and the built-in voltages of the junction; $N_{\rm np}$ is the carrier concentration in the NBG region and is equal to $N_{\rm bp}$ here; $V_{\rm Dnp}$ is the built-in voltage of the NBG region; $\Delta E_{\rm F}$ is the Fermi level difference between the NBG and the BBG regions; $\varepsilon_{\rm n}$ and $\varepsilon_{\rm b}$ are the dielectric constants of the material, which are related by

$$\varepsilon = (3.59 - 0.7x + 0.09x^2)^2 \varepsilon_0. \tag{16}$$

In the case of complete ionization of impurity, $\Delta E_{\rm F}$ can be expressed as

$$\begin{aligned}\Delta E_{\rm F} &= \Delta E_{\rm v} + \frac{3}{2}kT\ln\left(\frac{m^*_{\rm hn}}{m^*_{\rm hb}}\right) - kT\ln\left(\frac{N_{\rm np}}{N_{\rm bp}}\right) \\ &= \Delta E_{\rm v} + \frac{3}{2}kT\ln\left(\frac{m^*_{\rm hn}}{m^*_{\rm hb}}\right),\end{aligned} \tag{17}$$

where $m^*_{\rm hn}$ and $m^*_{\rm hb}$ are the effective masses of the holes in both the NBG and BBG regions of the junction, respectively; $\Delta E_{\rm v}$ denotes the valence-band difference between the NBG and the BBG regions and can be expressed as

$$\Delta E_{\rm v} = 0.3\Delta E_{\rm g}, \tag{18}$$

$$\Delta E_{\rm g} = \begin{cases} 1.247\Delta x, & x < 0.45, \\ 1.247\Delta x + 1.147(x + \Delta x - 0.45)^2 \\ -1.147(x - 0.45)^2, & x > 0.45. \end{cases} \tag{19}$$

Equation (9) indicates that with the increase of applied voltage, the junction resistance of the reverse-bias junction increases rapidly, while that of the forward-bias junction varies a little so that its influence may be omitted in the resistance analysis. Thus, the resistance of the reverse-bias junction in one pair of DBR layers will play a dominant role in the DBR resistance effect. This is illustrated in Fig. 3.

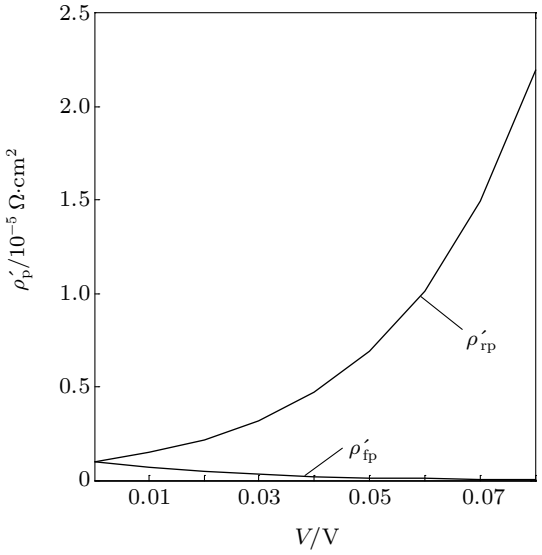


Fig. 3. Differential resistances versus voltage applied to the forward-bias and reverse-bias junctions in a pair of DBR layers.

3.2. Junction resistance of the graded n-DBR

For the n-type DBR mirror, the Fermi level difference between the NBG and the BBG regions is written as

$$\begin{aligned}\Delta E_{\rm F} &= \Delta E_{\rm c} - \frac{3}{2}kT\ln\left(\frac{m^*_{\rm nn}}{m^*_{\rm nb}}\right) - kT\ln\left(\frac{N_{\rm nn}}{N_{bn}}\right) \\ &= \Delta E_{\rm c} - \frac{3}{2}kT\ln\left(\frac{m^*_{\rm nn}}{m^*_{\rm nb}}\right),\end{aligned} \tag{20}$$

$$\Delta E_{\rm c} = 0.7 \cdot \Delta E_{\rm g}, \tag{21}$$

where $m^*_{\rm nn}$ and $m^*_{\rm nb}$ are the effective masses of the electrons in the NBG and BBG regions of the n–n junction; $\Delta E_{\rm c}$ denotes the conduction-band difference between the NBG and BBG regions; $N_{\rm bn}$ and $N_{\rm nn}$ are the carrier concentrations in the BBG and NBG regions and are approximately equal to the impurity concentrations in the material system.

The equations for the p-DBR resistance calculation in Subsection 3.1 can still be used for the n-DBR resistance calculation, as long as the concentration and the effective mass of the hole for the p-DBR are replaced by electron parameters for the n-DBR. In general, the effective mass of the electron is much less than that of the hole, so it would be an important

influence on reducing the junction resistance of the n-DBR. However, the voltage applied to the DBR mirror would be another influence that cannot be omitted in the resistance analysis. Thus, in order to assess the junction resistances of both p- and n-DBRs, the resistances of each as a function of applied voltage are plotted in Fig. 4, in which the voltage drops across the active region, the substrate and both electric contacts are ignored due to their resistances being much lower than the DBR when lasing is generated,[9,14] that is, $V = V_{\rm p} + V_{\rm n}$. The finite different number for dividing one layer of the DBR into a number of transitional sub-layers is set to be $n = 20$ in the calculation. The applied voltage V at the threshold of the VCSEL is used to reduce the thermal influence, which is 1.6 V from Fig. 2.

Figure 4 clearly shows that the junction resistance of the n-DBR mirror cannot be simply omitted, in comparison with the resistance of p-DBR, even if the voltages applied to the p- and n-DBRs are 1.6 V and zero, respectively. This illustrates that both the p- and n-DBR resistances should be taken into account for the graded DBR mirrors. In addition, the resistance of the p-DBR mirror is more sensitive to the voltage applied to it.

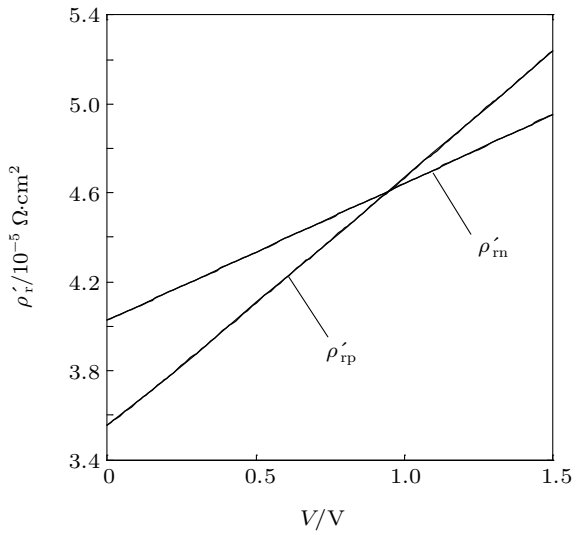


Fig. 4. Junction resistances versus applied voltage with a finite difference number of $n = 20$ for both DBRs.

In order to investigate the resistance minimized in the graded DBR mirrors, various voltages and finite different numbers are used in the resistance calculations of both p- and n-DBR mirrors, as it is actually difficult to exactly determine the voltage applied to each DBR mirror by modeling or in experiments. However, these voltages should meet the condition of $V = V_{\rm p} + V_{\rm n}$. With Eq. (9), the resistances, $\rho'_{\rm rp}$ and $\rho'_{\rm rn}$ each as a function of finite difference number, n, are obtained and plotted in Fig. 5.

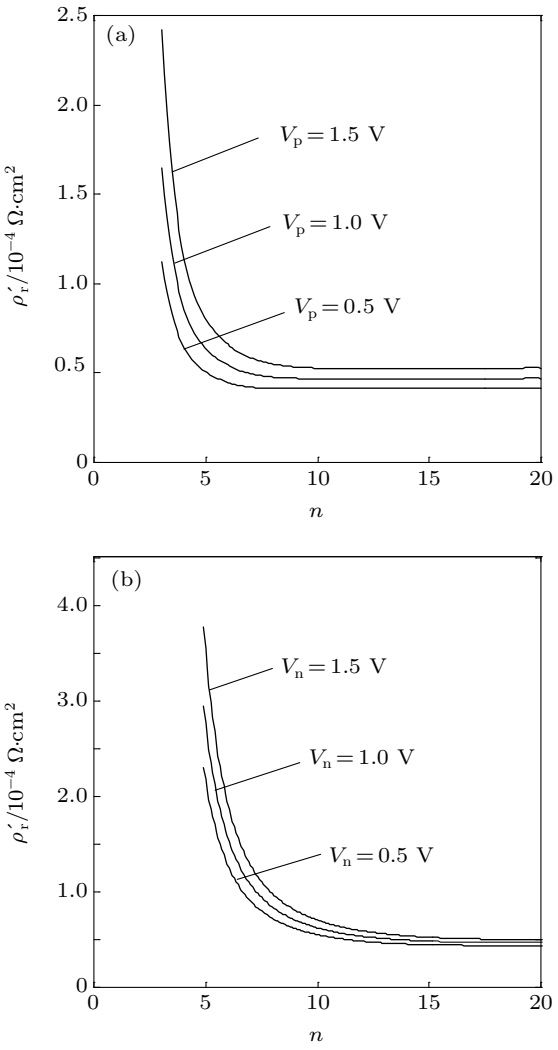


Fig. 5. Junction resistances of the p-DBR layer (a) and the n-DBR layer (b) versus the finite difference number at three different applied voltages.

The results from Fig. 5 show that with the increase of the finite difference number, i.e., the number of the transitional sub-layers within one DBR layer, the junction resistance of the p- or n-DBR mirror is significantly reduced and eventually stabilizes and approaches the minimal value. This means that the minimal resistance of the DBR mirror may be obtained by using finite discrete transitional layers in one DBR layer, and it can be equivalent to the resistance of the continuously-graded DBR layer. The calculation result also shows a quantitative relationship between junction resistance and the transitional sub-layer number of one layer. This is helpful for optimizing the design and fabrication of the graded DBR mirrors.

4. Temperature dependence and distribution of DBR resistances

With the above model, the differential resistances of both p- and n-DBRs can be obtained as 5.24×10^{-5} $\Omega\cdot\text{cm}^2$/pair and 4.09×10^{-5} $\Omega\cdot\text{cm}^2$/pair, provided that the voltages applied to the p- and n-DBRs are 1.5 V and 0.1 V, respectively, where the overall voltage drop of the device is 1.6 V. If the device is 800 μm in diameter, the series junction resistances of the p- and n-type DBR mirrors will be 0.31 Ω and 0.23 Ω, respectively, and the series intrinsic resistances of the p- and n-type DBR mirrors will be 3.37×10^{-4} Ω and 1.1×10^{-5} Ω, respectively. Thus, the overall series resistance including both intrinsic and junction resistances of the two DBRs will be 0.52 Ω. This value is slightly smaller than the overall device resistance of about 0.6 Ω from the L–I–V data of the sample, as the resistances of both the top and bottom contacts in the active region and the substrate are omitted in the calculation.

Obviously, the above results show that the intrinsic resistances of both DBR mirrors can be omitted in the following calculation, in comparison with the junction resistances. With Eqs. (9)–(21), the junction resistances each as a function of temperature can be calculated and plotted in Fig. 6.

It is clearly seen from Fig. 6 that the resistance is reduced with the increase of temperature in the DBR mirrors. This can be understood by the following physical process. As the temperature in the material increases, the bandgap of the material decreases[15] and the carrier energy increases. This leads the effective barrier height or the bandgap difference between two sides of the junction to decrease so that it is easier for carriers to diffuse into the junction under the same bias voltage. As a result, the differential resistance of the junction becomes smaller.

Since a Gaussian-like function may be used for describing the radial temperature distribution in the VCSEL from the data,[16–18] a temperature function $T(r) = 101\text{e}^{-1.83\times10^{-4}r^2} + 302$ is assumed here as an example, which is obtained from the fit to the data in Ref. [18] to investigate the temperature-induced radial variation of the DBR resistance. Thus, the radial junction resistance distributions of the DBRs due to the different temperatures can be described in Fig. 7.

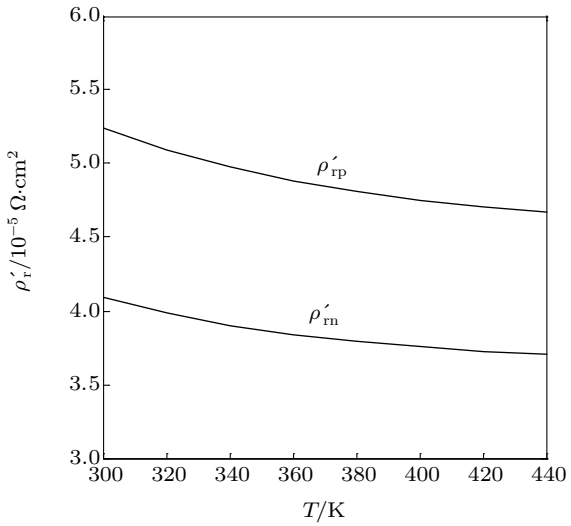


Fig. 6. Junction resistances versus temperature for the graded p- and n-DBR mirrors.

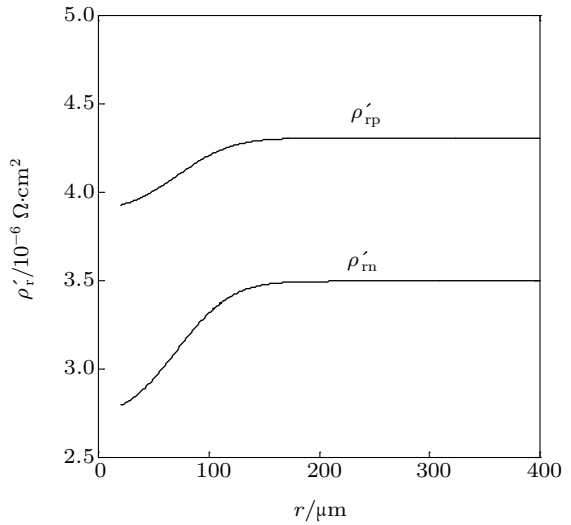


Fig. 7. Radial junction resistance distributions due to different temperatures in both DBRs.

The result from Fig. 7 shows that the central resistance is actually lower than that on the side in the DBR mirror resulting from the temperature influence. Thus, the DBR resistance cannot be simply treated as a constant for the overall cross-section in the VCSEL. Such a resistance variation would play a reverse role in Ohm heating.

5. Conclusions

The resistance characteristics of the DBR which has a continuously-graded barrier in a 980-nm vertical-cavity surface-emitting laser (VCSEL) are modeled. The junction resistance between the layers of both p- and n-DBR mirrors is analysed in detail by combining the thermionic emission model and the finite

difference method. In the meantime, the intrinsic resistance of the DBR material system is calculated to make a comparison with the junction resistance. The minimal values of series resistances in the graded p- and n-type DBR mirrors and the lateral temperature-dependent resistance distribution are calculated and discussed. The modeling results show that (i) the intrinsic resistances of both DBR mirrors may actually be omitted in comparison with the junction resistances, (ii) the junction resistances of both the p- and n-DBR mirrors in the 980-nm VCSEL are comparable in value to each other so that the resistance of the n-DBR cannot be simply omitted in the design of the resistance-related electro-thermo-optic characteristics of the 980-nm VCSEL, (iii) the junction resistance of the p- or n-DBR mirror may be significantly reduced and eventually approach a stable value minimized by using a number of transitional layers which have different discrete x-values within one DBR layer. The result can be equivalent to the resistance of a continuously-graded DBR layer. The quantitative relationship between the junction resistance and the transitional layer number in one layer of the DBR is obtained. This is helpful for optimizing the design and fabrication of the graded DBR mirrors, (iv) there is a radial resistance distribution with the central resistance lower than the resistance on the side of the DBR mirror, owing to the temperature influence. Thus, the DBR resistance cannot be simply treated as a constant for the overall cross-section in the VCSEL in some cases.

References

[1] Chuang H H, Biard J R, Guenter J, Johnson R, Evans G A and Butler J K 2007 *IEEE J. Sel. Top. Quantum Electron.* **43** 1028

[2] Zhou P, Cheng J, Schaus C F, Sun S Z, Zheng K, Armour E, Hains C, Hsin W, Myers D R and Vawter G A 1991 *IEEE Photon. Technol. Lett.* **3** 591

[3] MacDougal, M H, Geske J, Lin C K, Bond A E and Dapkus P D 1998 *IEEE Photon. Technol. Lett.* **10** 9

[4] Tai K, Yang L, Wang Y H, Wynn J D and Cho A Y 1990 *Appl. Phys. Lett.* **56** 2496

[5] Nabiev R F, Chang H and C J 1995 *IEEE Photon. Technol. Lett.* **7** 733

[6] Modh P, Galt S, Gustavsson J, Jacobsson S and Larsson A 2006 *IEEE Photon. Technol. Lett.* **18** 100

[7] Kawakami T, Kadota Y, Kohama Y and Tadokoro T 1992 *IEEE Photon. Technol. Lett.* **4** 1325

[8] Lear K L and Chalmers S A 1993 *IEEE Photon. Technol. Lett.* **5** 972

[9] Duan X F, Zhang C, Zhou B and Xu C M 2002 *SPIE* **4913** 194

[10] Osinski M, Smagley V A, Min L, Smolyakov G A, Eliseev P G, Riely B P, Shen P H and Simonis G J 2003 *IEEE J. Sel. Top. Quantum Electron* **9** 1422

[11] Casey H C Jr and Panish M B 1978 *Heterostructure Lasers* Part A: *Fundamental Principles* (New York: Academic Press)

[12] Anderson R J 1962 *Solid State Electronics* **5** 341

[13] Kumar R C 1968 *Solid State Electronics* **11** 543

[14] Achtenhagen M, Hardy A A and Kapon E 2006 *IEEE J. Sel. Top. Quantum Electron.* **42** 891

[15] Tsai H M, Tang S F, Sua S T, Chen T C and Chiang C D 2007 *SPIE* **6484** 64840I

[16] Osinski M and Nakwaski W 1991 *JJAP* **30** 596

[17] Osinski M and Nakwaski W 1995 *IEEE J. Sel. Top. Quantum Electron.* **1** 681

[18] Wu J 2006 *Acta Phys. Sin.* **55** 5848 (in Chinese)